Reprinted from JOURNAL OF THE OPTICAL SOCIETY OF AMERICA, Vol. 57, No. 9, 1105–1114, September 1967
Printed in U. S. A.

Theory for Off-Specular Reflection From Roughened Surfaces*

K. E. TORRANCE†
National Bureau of Standards, Washington, D. C. 20234

AND

E. M. SPARROW
University of Minnesota, Minneapolis, Minnesota 55455

(Received 27 December 1966)

The directional distribution of radiant flux reflected from roughened surfaces is analyzed on the basis of geometrical optics. The analytical model assumes that the surface consists of small, randomly disposed, mirror-like facets. Specular reflection from these facets plus a diffuse component due to multiple reflections and/or internal scattering are postulated as the basic mechanisms of the reflection process. The effects of shadowing and masking of facets by adjacent facets are included in the analysis. The angular distributions of reflected flux predicted by the analysis are in very good agreement with experiment for both metallic and nonmetallic surfaces. Moreover, the analysis successfully predicts the off-specular maxima in the reflection distribution which are observed experimentally and which emerge as the incidence angle increases. The model thus affords a rational explanation for the off-specular peak phenomenon in terms of mutual masking and shadowing of mirror-like, specularly reflecting surface facets.

INDEX HEADINGS: Reflection; Radiometry; Geometrical optics.

IN the calculation of radiant interchange, rough surfaces are usually assumed to be diffuse reflectors. Recent experiments[1,2] have shown, however, that the diffuse distribution is approached with increasing surface roughness only when the incident flux arrives in a near-normal direction. At moderate and large angles of incidence, diffuse reflection is not approached as the surface roughness increases. Instead, a maximum in the distribution of the reflected radiance occurs at an angle (relative to the normal) larger than the specular angle.

Evidence of the off-specular peak phenomenon has frequently appeared in published reflectance data. A survey of pertinent contributions to the subject is presented elsewhere,[1] to which additional references may be appended.[2–4] Off-specular peaks have been observed for both metallic and nonmetallic surfaces[1]; an approximate criterion for their appearance is that the root-mean-square surface roughness σ_m is comparable to or greater than the wavelength of the incident radiant energy ($\sigma_m/\lambda \gtrsim 1.0$).

The present paper is aimed at providing a model of reflection by a rough surface which successfully predicts the experimental findings. Reflection of electromagnetic waves by a roughened reflecting surface can be studied analytically by using either physical or geometrical optics. The physical-optics (or wave-theory) approach has been applied to the scattering of radar waves from

* This paper is based on work done at the Heat Transfer Laboratory, University of Minnesota, Minneapolis, Minnesota.
† Currently Research Associate at the National Bureau of Standards, Washington, D. C. 20234 from Factory Mutual Engineering Corp., Norwood, Mass.
[1] K. E. Torrance and E. M. Sparrow, J. Heat Trans. **88**, Ser. C, 223 (1966).
[2] K. E. Torrance, E. M. Sparrow, and R. C. Birkebak, J. Opt. Soc. Am. **56**, 916 (1966).
[3] S. Tanaka, J. Applied Physics (Japan) **25**, 207 (1956); **26**, 85 (1957); **27**, 600, 758 (1958); **28**, 508 (1959).
[4] W. M. Brandenberg and J. T. Neu, J. Opt. Soc. Am. **56**, 97 (1966).

rough surfaces, and an excellent summary of the literature is available.[5] This approach is, in principle, capable of predicting the angular distribution of reflected flux and the dependence on angle of incidence and wavelength. Typically, however, it has been assumed that the reflecting surface is a perfect electrical conductor, and that the incident flux arrives from a near-normal direction so that multiple reflections and shadowing by surface asperities do not occur. Solutions which avoid the latter assumption have not been obtained, owing to the added complexity. As a result, none of the existing analytical models based on physical optics predict the observed off-specular peaks. Consequently, we concentrated on a model employing the mathematically simpler geometrical optics.

Geometrical optics makes use of the ray-like nature of light. It is generally able to explain the gross behavior of light when the wavelength is small compared with the pertinent physical dimensions of the system. Therefore, in the case of reflection by a rough surface, the ray theory is, strictly speaking, valid only when the surface roughness is large compared to the wavelength of the radiation ($\sigma_m/\lambda \gg 1$).

Two models based on geometrical optics have already been proposed to explain the off-specular peaks. These models were formulated in efforts to explain the off-specular peaks in the experimental data of the respective authors. The data were obtained in the plane of incidence[6] using visible light and roughened nonmetallic surfaces. Correspondingly, the models were essentially developed for, and applied in, the plane of incidence.

The first of such models, due to Pokrowski,[7] consists of specular reflection (obeying the Fresnel equation) from small mirror-like facets on the surface, plus a more or less diffuse scattering that originates both on the surface and internally. Pokrowski attributed the off-specular peaks to reflection from the facets. The resulting analytical representation has four arbitrary constants; these can be adjusted to provide a satisfactory fit for some of Pokrowski's reflection data for flux arriving at an angle of incidence $\psi=80°$. In all cases, however, the predicted distributions become infinite at $\theta=90°$. Such infinite values of reflectance are in sharp disagreement with experiment. [The zenith angles of incidence and reflection are measured from the surface normal and are respectively denoted by ψ and θ (see Fig. 1).]

Later, Schulz[8] modified the Pokrowski model by giving a statistical distribution of slopes to the mirror-like facets on the surface. In effect, this provides additional arbitrary constants. Schulz, however, did not fit the analytical model to his own data. It can be shown that the Schulz modification yields weak off-specular peaks, but the absolute maximum is still infinite and is at $\theta=90°$.

The more recent model of Middleton and Mungall[9] contains the mirror-like-facet and diffuse-scattering mechanisms of Pokrowski–Schulz, but also includes a multiplicative factor to account for the shadowing and masking of the elementary mirror-like facets by adjacent facets. The multiplicative factor causes the model to predict a finite value for the reflectance at $\theta=90°$, which is in better accord with experiment. The resulting equation has three arbitrary constants and, on the basis of numerical evaluations by Middleton and Mungall, appears to describe certain trends characteristic of their experimental data. For incidence at $\psi=75°$, the distributions calculated by Middleton and Mungall exhibit off-specular peaks at zenith angles $75°<\theta<90°$. However, at smaller angles of incidence, their calculated distributions display a maximum either at the specular angle or at $\theta=90°$. The off-specular peaks were attributed by these authors to the shape of the Fresnel reflection curve, their specific interest being in a nonmetal. If this view is accepted, then the model would not predict off-specular peaks for metals.[10]

For the aforementioned cases, where the distributions displayed a maximum at $\theta=90°$ for smaller incidence angles, we could not reproduce the off-specular maximum for incidence at $\psi=75°$ by numerical evaluation of the Middleton and Mungall model. Rather, the calculated reflectance distributions for $\psi=75°$ also displayed a maximum at $\theta=90°$. This was brought to the attention of Mungall, who, in a personal communication,[11] expressed the view that the calculations reported in the published paper[9] seem to be in error for the $\psi=75°$ cases just discussed.[12] Consequently, we conclude that the Middleton and Mungall model does not predict off-specular peaks of the type observed experimentally.

Thus, we conclude that both of the previously proposed models are deficient. That of Pokrowski and Schulz is unrealistic because it predicts infinite reflectance as θ approaches 90°. The Middleton and Mungall analysis on the other hand, exhibits significant departures from experiment. A model which overcomes these objections is developed in the following sections. The present analysis predicts the angular distribution of flux reflected throughout the entire hemisphere above the reflecting surface, and exhibits off-specular peaks for both metallic and nonmetallic surfaces. The formulation is based on geometrical optics and applies when $\sigma_m/\lambda \gg 1$. Before proceeding with the development of

[5] P. Beckmann and A. Spizzichino, *The Scattering of Electromagnetic Waves from Rough Surfaces* (Pergamon Press, New York, 1963).

[6] The plane of incidence includes the incident beam and the surface normal.

[7] G. I. Pokrowski, Z. Physik **30**, 66 (1924); **35**, 34 (1925); **35**, 390 (1926); **36**, 472 (1926).

[8] H. Schulz, Z. Physik **31**, 496 (1925).

[9] W. E. K. Middleton and A. G. Mungall, J. Opt. Soc. Am. **42**, 572 (1952).

[10] Fresnel reflectance curves for a metal and nonmetal are shown in Fig. 6 of this paper.

[11] A. G. Mungall (private communication, 23 September 1965).

[12] The original calculations were performed by hand; the present re-evaluation employed an electronic computer.

the model, we will present definitions and relevant experimental data.

DEFINITIONS AND COORDINATE SYSTEM

The angular distribution of reflected radiant flux is conveniently expressed in terms of the bidirectional reflectance. The designation "bidirectional" indicates that two directions are involved: the direction of incidence and the direction of reflection. The coordinate system used to describe these directions is shown in Fig. 1, which pictures the hemisphere above a reflecting surface element dA. The direction of the incident radiation is specified by its zenith angle ψ measured from the surface normal. The direction of the reflected flux requires specification of two angles: the zenith angle θ measured from the surface normal and the azimuthal angle ϕ measured from the plane of incidence. These angles are conveniently combined in the reflection triplet $(\psi;\theta,\phi)$, where the first angle denotes the incidence direction and the second and third specify the reflection direction. For surfaces of isotropic roughness, as assumed here, the reflection triplet is a sufficient description of the angular directions.

To facilitate the definition of bidirectional reflectance, we first define radiance (N). Radiance is the radiant flux (Φ) per unit solid angle (ω) in the direction of a ray per unit projected area $(A\cos\theta$ or $A\cos\psi)$ perpendicular to the ray. Thus, the radiant flux from a small source of radiance N_i in the direction of dA is

$$d\Phi_i(\psi)=N_i(\psi)\cos\psi dA\,d\omega_i, \tag{1a}$$

where $d\omega_i$ is the solid angle of the source when viewed from dA. On the other hand, the radiance of dA in the direction (θ,ϕ) due to reflection of radiation from this source is $dN_r(\psi;\theta,\phi)$.[13] This is designated dN_r to emphasize that it is associated with a small source. The reflected radiance N_r of dA in the direction (θ,ϕ) is then the integral of $dN_r(\psi;\theta,\phi)$ over all sources from which radiant flux is incident on the reflecting surface. If a small collector is placed so that it subtends a solid angle $d\omega_r$ when viewed from dA in the direction (θ,ϕ) then the radiant flux from the small source reflected by dA that is intercepted by the collector is

$$d\Phi_r(\psi;\theta,\phi)=dN_r(\psi;\theta,\phi)\cos\theta dA\,d\omega_r. \tag{1b}$$

The bidirectional reflectance is denoted here by the symbol ρ. It is defined as the reflected radiance (dN_r) in the direction (θ,ϕ) divided by the incident radiant flux from the small source per unit surface area $(d\Phi_i/dA)$; that is,

$$\rho(\psi;\theta,\phi)\equiv\frac{dN_r(\psi;\theta,\phi)}{d\Phi_i(\psi)/dA}=\frac{dN_r(\psi;\theta,\phi)}{N_i(\psi)\cos\psi d\omega_i}. \tag{2}$$

The reflectance defined by Eq. (2) has also been called biangular reflectance,[1,2,14] apparent unidirectional reflectance,[15] and partial reflectance.[16,17] We use the term bidirectional reflectance[14] because it clearly connotes the dependence on direction of illumination and direction of reflection. The definition of bidirectional reflectance represented by Eq. (2) leads to certain important reciprocal relations among reflectances.[14–17]

In the present application, the foregoing definitions are applied monochromatically.

EXPERIMENTAL REFLECTANCE DISTRIBUTIONS

To provide orientation for the forthcoming analytical development, it is useful to examine some representative, experimentally determined reflectance distributions. The emergence of the off-specular-peak phenomenon with increasing incidence angle ψ is illustrated in Fig. 2. This figure includes bidirectional reflectance distributions for both a metal and a nonmetal. Additional results and details of the experimental measurements are reported elsewhere.[1,18]

In the figure, the bidirectional reflectance in the direction θ is plotted relative to that in the specular direction $\theta=\psi$. The abscissa is the reflection angle θ and the curve parameter is the incidence angle ψ. Figure 2 is for the plane of incidence ($\phi=0°$ or $180°$); positive and negative abscissa values correspond to $\phi=0°$ and $\phi=180°$, respectively. This convention is used throughout the present work. Figures 2(a) and 2(b) apply to aluminum-coated aluminum and magnesium oxide ceramic specimens, respectively, at a wavelength $\lambda=0.5\,\mu$.

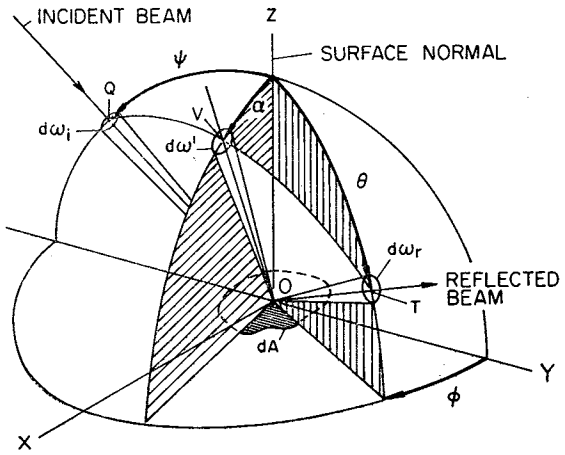

FIG. 1. Spatial angles of incident and reflected flux.

[13] The reflection triplet $(\psi;\theta,\phi)$ applies to quantities which depend on the angle of incidence and the angles of reflection. A single angle in parentheses is used for quantities which depend on only one angle.

[14] J. A. Clark, Ed., *Theory and Fundamental Research in Heat Transfer* (Pergamon Press, New York, 1963), p. 7.
[15] H. J. McNicholas, J. Res. Natl. Bur. Std. (U. S.) 1, 29 (1928).
[16] C. von Fragstein, Optik 12, 60 (1955).
[17] F. E. Nicodemus, Appl. Opt. 4, 767 (1965).
[18] K. E. Torrance, Ph.D. dissertation, University of Minnesota (March 1966).

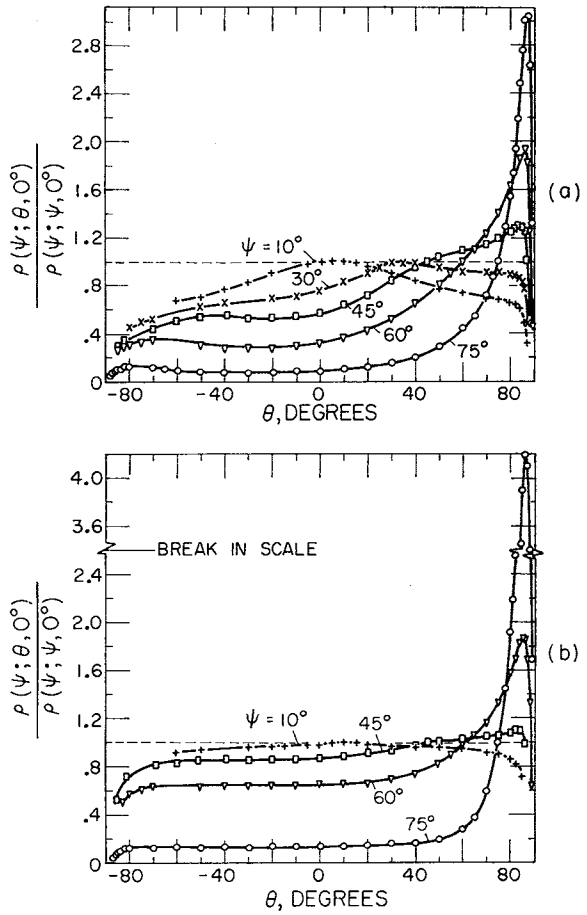

FIG. 2. Bidirectional reflectance distributions in the plane of incidence for various angles of incidence ψ, $\lambda = 0.5\ \mu$. (a) Aluminum (2024-T4), aluminum coated, $\sigma_m = 1.3\ \mu$. (b) Magnesium oxide ceramic, $\sigma_m = 1.9\ \mu$.

The aluminum specimen was taken from a bar of 2024-T4 alloy. After the surface was prepared, it was coated with a vacuum-deposited layer of very pure aluminum. The ceramic specimen is a high purity (99.9%) fused polycrystalline magnesium oxide ceramic supplied by Honeywell, Incorporated. The test surfaces were initially polished flat using a standard optical polishing technique. Subsequently, a similar technique was used to roughen the surfaces, using grinding grits of 31 μ diameter. Carborundum grit and aluminum oxide grit were used for the aluminum and magnesium oxide specimens respectively. The surface roughness of the test specimens was measured with a stylus profilometer (Taylor–Hobson Talysurf model 3). The measured surface roughness was $\sigma_m = 1.3\ \mu$ for aluminum and $\sigma_m = 1.9\ \mu$ for the ceramic.

The developing off-specular peaks shown in Fig. 2 are representative of the case in which the surface roughness is comparable to or larger than the wavelength of the radiation ($\sigma_m/\lambda \gtrsim 1.0$). In the type of presentation employed here, an ideal diffuse surface (i.e., one which obeys Lambert's cosine law of reflection) would have a constant value of the relative bidirectional reflectance equal to 1.0. Thus, the deviation of any of the curves from the dashed reference line, drawn at an ordinate of unity, is a measure of how they differ from the ideal diffuse limit.

The results for near-normal incidence, $\psi = 10°$, resemble the diffuse limit. As the angle of incidence increases, it is apparent that the corresponding reflectance distributions differ markedly from that for a diffuse surface. For incidence at $\psi = 45°$, the distributions display a maximum in the region $\theta = 80°$ to 85°. As ψ increases still further, the maxima in the vicinity of $\theta = 85°$ grow rapidly in magnitude, until, at $\psi = 75°$, the off-specular peak dominates the distribution. Moreover, this off-specular maximum is quite different in shape from the sharp, specular-reflection maximum occurring at $\theta = \psi$ on a smoother surface. It is thus evident that the diffuse distribution is approached only when the angle of incidence is near normal.

DEVELOPMENT OF THE THEORY

Formulation of the Model

Reflection from a roughened surface is assumed to be composed of two components: specular reflection from mirror-like surface facets—a function of the angles of reflection, and a diffuse component—independent of angles of reflection. The diffuse component may originate either from multiple reflections among the facets and/or from internal scattering, while the specular component is subject to mutual shadowing and masking by adjacent facets.

The reflected flux is thus pictured as being composed of a uniformly scattered component plus a perturbation due to the mirror-like facets. Clearly, this initial premise associates the off-specular peaks with specular reflection from the facets. This model of reflection is in general accord with measurements of the state of polarization of light reflected from rough surfaces.[2,3,19,20] In the development that follows, cognizance has also been taken of the suggestions of Christie.[21]

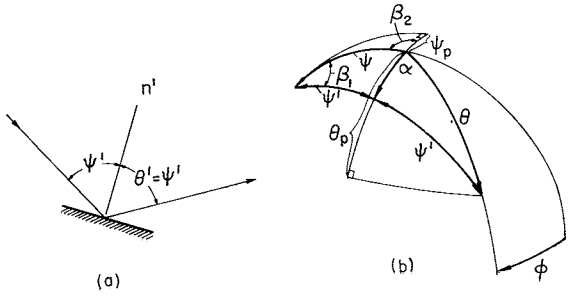

FIG. 3. (a) Reflection at a mirror-like facet. (b) Spherical triangle of reflection.

[19] G. M. Gorodinskii, Opt. Spectry. **16**, 59 (1964).
[20] V. K. Polyanskii and V. P. Rvachev, Opt. Spectry. **20**, 391 (1966).
[21] A. W. Christie, J. Opt. Soc. Am. **43**, 621 (1953).

The just-discussed composition of the reflected flux is expressed as

$$dN_r(\psi;\theta,\phi)=dN_{r,s}(\psi;\theta,\phi)+dN_{r,d}(\psi). \quad (3)$$

The differential notation dN_r, $dN_{r,s}$ and $dN_{r,d}$ is used to emphasize that these quantities are associated with a small radiant source. If a source of constant radiance N_i is oriented at various angles of incidence ψ, the diffuse component of reflected flux will vary directly as the cosine of the angle ψ. This is because the flux incident on a unit area of surface varies as $\cos\psi$. Thus,

$$dN_{r,d}(\psi)=aN_i\cos\psi, \quad (4)$$

where a is a constant.

The angular dependence of the flux that is specularly reflected from the elementary mirrors is not so easily determined. First, consider flux reflected from the single mirror-like facet shown in Fig. 3(a). Flux impinges at an angle ψ' with respect to the normal n' of the facet surface. Specular reflection occurs in the direction $\theta'=\psi'$. In general, the angles ψ' and θ' are different from the angles ψ and θ, the latter being measured with respect to the normal n of the mean surface dA. To proceed, it is necessary to relate these pairs of angles.

Consider, as is illustrated in Fig. 1, an element of surface dA which is illuminated by a source of radiance N_i subtending a solid angle $d\omega_i$ when viewed from a point O in dA. Let Q be a point on the intersection of $d\omega_i$ with the unit sphere. Similarly, imagine that reflected flux is collected within a solid angle $d\omega_r$ and that point T lies on the unit sphere within $d\omega_r$. The normals of the facets at O which can specularly reflect flux incident from Q into $d\omega_r$ lie in an elementary solid angle $d\omega'$ containing the line OV which bisects the angle QOT. The angle QOV is the angle of incidence with respect to the facets, ψ', and the angle VOT is the facet reflection angle θ'. The facet normals are inclined at an angle $VOZ=\alpha$ with respect to the normal of the mean surface.

Let $Pd\omega'$ be the number of facets per unit surface area, whose normals are contained within $d\omega'$. For isotropic surfaces, a gaussian probability distribution for P with rotational symmetry about the surface normal OZ may be assumed, that is,

$$P=P(\alpha)=b\exp(-c^2\alpha^2), \quad (5)$$

where b and c are constants.

The number of facets in dA with normals lying within $d\omega'$ is

$$P(\alpha)d\omega' dA.$$

Assuming each facet to be of area f, the total reflecting area of the facets is

$$fP(\alpha)d\omega' dA$$

and the projection of this area in the direction of the source is

$$f\cos\psi' P(\alpha)d\omega' dA.$$

The incident radiance N_i is the radiant flux per unit projected area and per unit solid angle, Eq. (1a). Thus, the flux incident upon the facets whose normals lie within $d\omega'$ is given by

$$d\Phi_i=fN_i\cos\psi' P(\alpha)d\omega' dA\,d\omega_i. \quad (6)$$

The surface is not a perfect reflector, hence, only a fraction of the flux reaching the facets is reflected. This fraction is given by the Fresnel reflectance $F(\psi',\hat{n})$ where $\hat{n}$ is the complex index of refraction of the material for normal incidence. The complex index $\hat{n}$ can be expressed in terms of the real index of refraction, n, and the coefficient of absorption, k, as $\hat{n}=n-ik$. The function $F(\psi',\hat{n})$ is calculated from the Fresnel equation.[22] Thus, the flux reflected from the facets with normals in $d\omega'$ is

$$F(\psi',\hat{n})d\Phi_i. \quad (7)$$

So far, masking and shadowing of one facet by adjacent facets has been neglected. Adjacent facets may obstruct either the flux incident upon a given facet or the flux reflected from it. Clearly, this will be a function of the angle of incidence and the angles of reflection. The analytical representation of the masking and shadowing factor G will be derived in the next section. For the present, it suffices to say that G depends only on the projections of ψ and θ onto the plane determined by the facet normal and the surface normal. These projections are denoted by ψ_p and θ_p and are shown in Fig. 3(b). The factor $G(\psi_p,\theta_p)$ is the fraction of an illuminated facet that actually contributes to the reflected flux. It will henceforth be referred to as the geometrical attenuation factor. Thus, the flux specularly reflected from the element of area is

$$\begin{aligned}d\Phi_r&=G(\psi_p,\theta_p)F(\psi',\hat{n})d\Phi_i\\&=fN_iG(\psi_p,\theta_p)F(\psi',\hat{n})\cos\psi' P(\alpha)d\omega' dA\,d\omega_i. \quad (8)\end{aligned}$$

The reflected radiance $dN_{r,s}(\psi;\theta,\phi)$ represents the specularly reflected radiant flux per unit projected surface area and per unit solid angle; see Eq. (1b). The elementary contribution to the flux specularly reflected from the element of area dA, in the elementary solid angle $d\omega_r$, can be expressed in terms of $dN_{r,s}$ as

$$d\Phi_r=dN_{r,s}(\psi;\theta,\phi)\cos\theta dA\,d\omega_r. \quad (9)$$

The elementary quantities of flux expressed by Eq. (8) and (9) are equal, and also[23]

$$d\omega'=d\omega_r/4\cos\psi', \quad (10)$$

so that

$$\begin{aligned}&dN_{r,s}(\psi;\theta,\phi)\\&\quad=(fN_id\omega_i/4)F(\psi',\hat{n})[G(\psi_p,\theta_p)/\cos\theta]P(\alpha). \quad (11)\end{aligned}$$

This can then be combined with Eqs. (3), (4), and (5)

[22] S. Flugge, ed., *Handbuch der Physik* (Springer-Verlag, Berlin, 1928), Vol. 20, pp. 240–250.

[23] W. A. Rense, J. Opt. Soc. Am. **40**, 55 (1950).

to yield

$$dN_r(\psi;\theta,\phi)=(bfN_i d\omega_i/4)F(\psi',\hat{n})[G(\psi_p,\theta_p)/\cos\theta]\times\exp(-c^2\alpha^2)+aN_i\cos\psi. \quad (12)$$

The bidirectional reflectance can now be evaluated. Using Eq. (2), we find the ratio of the bidirectional reflectance $\rho(\psi;\theta,\phi)$ to that in the specular direction of the mean surface $\rho(\psi;\psi,0°)$,

$$\frac{\rho(\psi;\theta,\phi)}{\rho(\psi;\psi,0°)}=\frac{dN_r(\psi;\theta,\phi)}{dN_r(\psi;\psi,0°)}=\frac{gF(\psi',\hat{n})[G(\psi_p,\theta_p)/\cos\theta]\exp(-c^2\alpha^2)+\cos\psi}{gF(\psi,\hat{n})[G(\psi,\psi)/\cos\psi]+\cos\psi}, \quad (13)$$

since $\alpha=0°$ when $\theta=\psi$ and $\phi=0°$. The letter g denotes an adjustable constant which determines the relative contributions of the two assumed modes of reflection: specular reflection from the mirror-like surface facets and diffuse reflection. Indeed, the former mode dominates when g is large and the latter mode exists alone when $g=0$.

The angles ψ', α, ψ_p, and θ_p are related to ψ, θ, ϕ, through the fundamental spherical triangle of reflection defined by Fig. 1 and shown in Fig. 3(b). Spherical trigonometry gives the following relations:

$$\psi'=\tfrac{1}{2}\cos^{-1}[\cos\theta\cos\psi-\sin\theta\sin\psi\cos\phi],$$
$$\alpha=\cos^{-1}[\cos\psi\cos\psi'+\sin\psi\sin\psi'\cos\beta_1], \quad (14)$$
$$\psi_p=\tan^{-1}[\cos\beta_2\tan\psi], \quad \theta_p=\psi_p+2\alpha,$$

where

$$\beta_1=\sin^{-1}[\sin\phi\sin\theta/\sin 2\psi'],$$
$$\beta_2=\pi-\sin^{-1}[\sin\beta_1\sin\psi'/\sin\alpha].$$

In the plane of incidence, Eqs. (14) simplify to

$$\psi'=(\psi+\theta)/2, \quad \alpha=(\theta-\psi)/2, \quad \psi_p=\psi, \quad \theta_p=\theta. \quad (15)$$

By applying Eqs. (14), we can evaluate the bidirectional reflectance ratio expressed by Eq. (13) for any direction in the hemisphere above the reflecting surface.

The Geometrical Attenuation Factor

The geometrical attenuation (masking and shadowing) factor is derived here under the following assumptions: (1) Each specularly reflecting facet comprises one side of a symmetric V-groove cavity. (2) The longitudinal axis of the cavity is parallel to the plane of the mean surface. (3) All azimuthal orientations of the longitudinal axis of the cavity are assumed equally probable. (4) All masking and shadowing effects take place within the cavities; this is equivalent to assuming that the upper edges of all V-groove cavities lie in the same plane. (5) Only the first reflection of an incident beam is added to the specularly reflected flux. (6) All multiple reflections are assumed to be perfectly diffused.

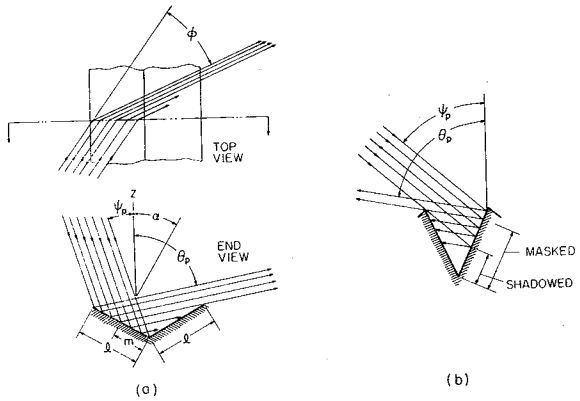

FIG. 4. (a) Geometry of the V-groove cavity. (b) Simultaneous masking-shadowing.

The geometry of the cavity is depicted in Fig. 4(a). Inspection of the top view reveals that, in general, the plane containing the incident and reflected beams makes a transverse cut across the cavity axis. However, the projection of the path of the flux onto a plane perpendicular to the cavity axis [end view of Fig. 4(a)] is sufficient for the formulation of the masking and shadowing effect. The plane perpendicular to the cavity axis includes the normals to the cavity walls and to the plane of the mean surface. Thus, the projection angles ψ_p and θ_p introduced in the previous section are the appropriate defining angles for the incident and reflected beams. In this connection, it is worthwhile to reiterate that ψ_p and θ_p are completely determined [Eqs. (14)] as soon as ψ, θ, and ϕ are specified.

The derivation that follows is carried out in the plane containing ψ_p and θ_p, and for convenience, ψ_p is always assumed positive. To avoid introducing an azimuthal reflection angle, values of θ_p and α as shown in Fig. 4(a) are assumed positive, that is, positive values are measured clockwise from the z axis.

FIG. 4(a) illustrates the case in which part of the flux reflected from a fully illuminated facet is intercepted by the adjoining face of the cavity. Such blockage of the specularly reflected energy will be called **masking**. Reversing the flux path in Fig. 4(a) illustrates the case in which the reflecting facet is only partially illuminated. Such an effect will be called **shadowing**. A third possibility exists, as shown in Fig. 4(b), for the case of large incidence angles ψ_p and large negative reflection angles θ_p, such that simultaneous **masking-shadowing** can occur.

The geometrical attenuation factor $G(\psi_p,\theta_p)$ is the fraction of the facet surface that contributes to the reflected flux. From Fig. 4(a), G can be defined as

$$G(\psi_p,\theta_p)=1-(m/l). \quad (16)$$

A value of G less than unity is caused by masking when the flux path is as shown in Fig. 4(a), by shadowing when the flux path is reversed, and by masking-shadowing when the flux path is as shown in Fig. 4(b).

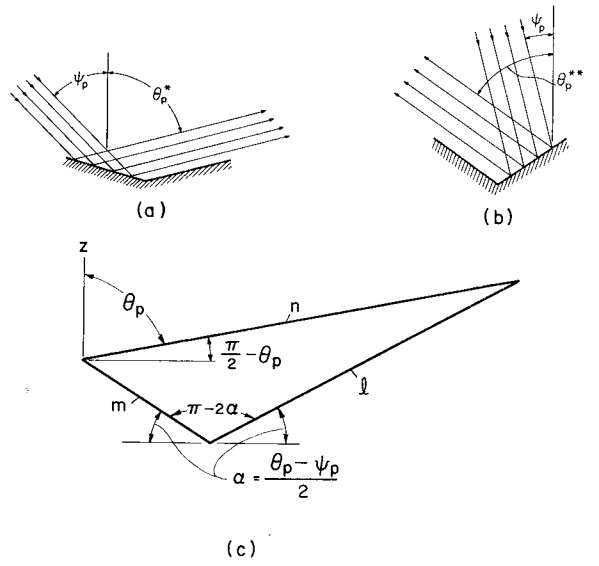

FIG. 5. (a) and (b) Illustration of the reflection angles θ_p^* and θ_p^{**}, respectively. (c) Reflection triangle for V-groove cavity.

For a given ψ_p, a range of reflection angles θ_p exists for which $G=1$ and none of the flux is obstructed. The limits of this range are denoted by θ_p^* and θ_p^{**}.

For all incidence angles ψ_p, there is a masking region at positive θ_p values between θ_p^* and $\pi/2$. The θ_p^* corresponds to the condition that the reflected beam is just parallel to the face of the adjoining cavity wall. This situation is shown in Fig. 5(a), and θ_p^* is given by

$$\theta_p^* = (\psi_p + \pi)/3. \tag{17}$$

For θ_p^{**}, on the other hand, consideration must be given to two ranges of ψ_p: $0 \leq \psi_p \leq \pi/4$ and $\pi/4 < \psi_p \leq \pi/2$. For each of these ranges, an equation for θ_p^{**} will be derived.

For angles of incidence $\psi_p \leq \pi/4$, there is a region that is either masked or masked-shadowed at negative θ_p values between $-\pi/2$ and θ_p^{**}. Since the angle at which the reflected beam is inclined has a magnitude greater than the angle of inclination of the incident beam, the value of θ_p^{**} is found from the condition that the reflected beam must be parallel to the face of the adjoining cavity wall. This is shown in Fig. 5(b), and θ_p^{**} is given by

$$\theta_p^{**} = (\psi_p - \pi)/3. \tag{18}$$

Consideration is next given to determining θ_p^{**} for the range $\pi/4 < \psi_p \leq \pi/2$. For $-\psi_p \leq \theta_p \leq \theta_p^{**}$, the incident beam has a greater inclination than the reflected beam, and shadowing occurs. The value of θ_p^{**} can be obtained from Eq. (17) by reversing the flux path and substituting ψ_p for θ_p^* and θ_p^{**} for ψ_p. Thus,

$$\theta_p^{**} = 3\psi_p - \pi. \tag{19}$$

In the range of angles $\theta_p^* < \theta_p \leq \pi/2$ and $-\pi/2 \leq \theta_p < \theta_p^{**}$, masking and/or shadowing will occur and $G<1$. In particular, when $\theta_p > \theta_p^*$, only masking occurs. For the case of $\theta_p < \theta_p^{**}$, we must separately consider the ranges $\psi_p \leq \pi/4$ and $\pi/4 < \psi_p \leq \pi/2$, as in the foregoing. In the first of these ranges, either pure masking or a masking–shadowing can occur; however, the masked region will always be the larger and the value of G can thus be determined as if masking occurred alone. In the second of these ranges, different conditions prevail when $-\psi_p \leq \theta_p < \theta_p^{**}$ and when $-\pi/2 \leq \theta_p < -\psi_p$. For the former, pure shadowing occurs; while for the latter, masking–shadowing occurs, with the masking region being dominant.

When masking exists alone or dominates, the expression for G may be derived by utilizing the triangle shown in Fig. 5(c). From the law of cosines

$$n^2 = m^2 + l^2 - 2ml\cos[\pi + \psi_p - \theta_p]. \tag{20a}$$

By projecting the sides of the triangle onto the horizontal, we find

$$n\cos[(\pi/2) - \theta_p] = (l+m)\cos[(\theta_p - \psi_p)/2]. \tag{20b}$$

Elimination of n^2 leads to a quadratic equation for m/l, the solution of which yields

$$G(\psi_p, \theta_p) = 1 - (m/l) = 1 - [1 - (1 - A^2)^{\frac{1}{2}}]/A, \tag{21a}$$

where

$$A = \frac{\sin^2\theta_p - \cos^2[(\theta_p - \psi_p)/2]}{\cos^2[(\theta_p - \psi_p)/2] - \cos[\theta_p - \psi_p]\sin^2\theta_p}. \tag{21b}$$

The negative square root was selected so that G is positive. When Eqs. (17) and (18) are inserted into (21b), it can be shown that $A=0$. Introduction of this result into Eq. (21a) leads to an indeterminate form for G. This can be resolved by using L'Hospital's rule, with the result that $G=1$ when $A=0$, thereby verifying the internal consistency of the derivation. At $\theta_p = \pm\pi/2$, $A=1$ and $G=0$ in accordance with physical boundary conditions.

In the case when shadowing occurs alone, G is derived from Eqs. (21) by replacing ψ_p by θ_p and θ_p by ψ_p. When Eq. (19) is introduced into the thus-modified Eqs. (21), it follows that $A=0$ and $G=1$. At $\theta_p = -\psi_p$, the values predicted by the original and modified forms of Eqs. (21) are identical. Thus, the internal consistency of the entire derivation is verified. The appropriate calculation formulas and their regions of application are summarized in Table I.

It has been noted in the foregoing that $G \to 0$ as $\theta_p \to \pm\pi/2$. Eq. (13) for the bidirectional reflectance ratio contains the quantity $G/\cos\theta$. As $\theta_p \to \pm\pi/2$, we see from Fig. 3(b) that the angle $\theta \to \pi/2$ and correspondingly, $\cos\theta$ approaches zero. It can be shown[18] that $G/\cos\theta$ approaches a finite limit as $\theta \to \pi/2$, given by

$$\lim_{\theta \to \pi/2} [G(\psi_p, \theta_p)/\cos\theta] = 2\cot\alpha/\cos(\beta_2 - \phi), \tag{22}$$

where β_2 is given in Eqs. (14).

TABLE I. Calculation formulas for the geometrical attenuation factor $G(\psi_p,\theta_p)$.

Incidence angle $0\leq\psi_p\leq\pi/4$		Incidence angle $\pi/4\leq\psi_p\leq\pi/2$	
Reflection angle	Formula	Reflection angle	Formula
$-\pi/2\leq\theta_p\leq\frac{\psi_p-\pi}{3}$	Eqs. (21)	$-\pi/2\leq\theta_p\leq-\psi_p$	Eqs. (21)
		$-\psi_p\leq\theta_p\leq3\psi_p-\pi$	Eqs. (21) with ψ_p and θ_p interchanged
$\frac{\psi_p-\pi}{3}\leq\theta_p\leq\frac{\psi_p+\pi}{3}$	$G(\psi_p,\theta_p)=1$	$3\psi_p-\pi\leq\theta_p\leq\frac{\psi_p+\pi}{3}$	$G(\psi_p,\theta_p)=1$
$\frac{\psi_p+\pi}{3}\leq\theta_p\leq\pi/2$	Eqs. (21)	$\frac{\psi_p+\pi}{3}\leq\theta_p\leq\pi/2$	Eqs. (21)

PREDICTED REFLECTANCE DISTRIBUTIONS

Directional distributions calculated from the just-described model will now be presented and compared with those of experiment. The experimental results shown in Fig. 2 are representative of a larger body of data[1,18] and display the significant characteristics for both metals and nonmetals. Consequently, the prediction of reflectance distributions compatible with Fig. 2 will be the goal of the following paragraphs.

The foregoing analysis of reflection leads to the bidirectional reflectance given by Eq. (13). Using $G(\psi,\psi)=1$, we find that Eq. (13) becomes

$$\frac{\rho(\psi;\theta,\phi)}{\rho(\psi;\psi,0°)}=\frac{gF(\psi',\hat{n})[G(\psi_p,\theta_p)/\cos\theta]\exp(-c^2\alpha^2)+\cos\psi}{g[F(\psi,\hat{n})/\cos\psi]+\cos\psi}. \quad (23)$$

For a given angle of incidence ψ and a given material, the only quantities dependent on the reflection angles are those appearing in the first term of the numerator, that is,

$$F(\psi',\hat{n})[G(\psi_p,\theta_p)/\cos\theta]\exp(-c^2\alpha^2). \quad (24)$$

This factor is presumably responsible for the observed off-specular peaks, and its behavior will now be investigated in detail.

The first ingredient of (24) is the Fresnel reflectance $F(\psi',\hat{n})$, which is shown in Fig. 6 for magnesium oxide and evaporated aluminum. The index of refraction $\hat{n}$ at wavelengths $\lambda=0.5\ \mu$ and $4.0\ \mu$ was obtained from the literature.[24] Fig. 6 reveals that the shapes of the Fresnel reflectance curves for aluminum are quite different from those of magnesium oxide. Such differences of shape are commonly observed when Fresnel curves for metals and nonmetals are compared. Since off-specular peaks are observed for metals as well as for nonmetals, it may be concluded that the Fresnel reflectance $F(\psi',\hat{n})$ cannot, in itself, be the cause of the peaks.

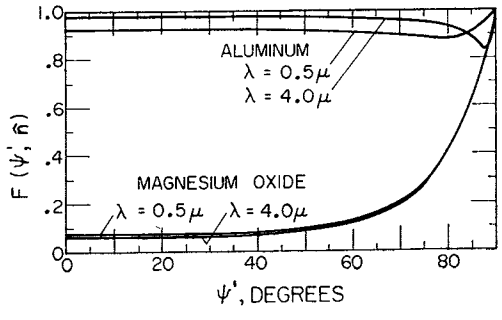

FIG. 6. Fresnel reflectance.

The third factor in (24), $\exp(-c^2\alpha^2)$, also cannot, in itself, cause the peaks. The exponential attains a maximum value of unity at the angle $\alpha=0°$, and is symmetric about that point. The angle $\alpha=0°$ corresponds to facets which lie parallel to the mean-surface plane and c determines the distribution of facet slopes about that plane. Moreover, $\alpha=0°$ corresponds to reflection

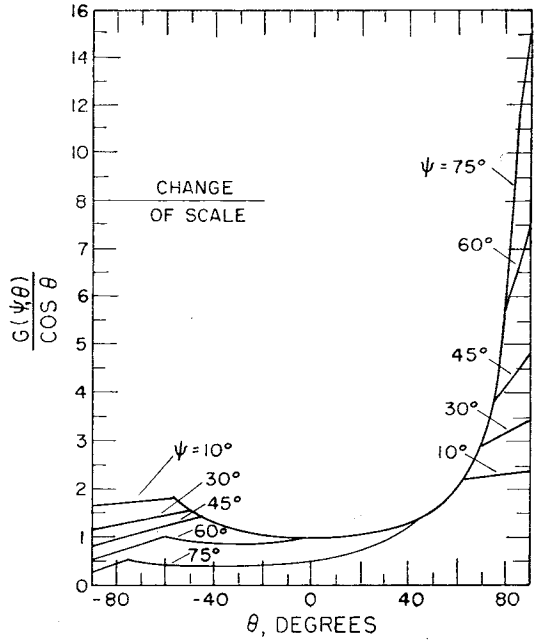

FIG. 7. The factor $G(\psi,\theta)/\cos\theta$ in the plane of incidence for various incidence angles ψ.

[24] *American Institute of Physics Handbook* (McGraw-Hill Book Co., New York, 1963), Second ed., pp. 6–12 and 6–107.

in the specular-ray direction $\theta=\psi$. At angles away from $\alpha=0°$, the exponential is less than unity, and the product $(G/\cos\theta)\exp(-c^2\alpha^2)$ could cause off-specular peaks only if $G/\cos\theta$ displayed a suitable behavior.

The quantity $G/\cos\theta$ must, therefore, be the key factor which causes Eq. (23) to attain values greater than unity. It is interesting to note that $G/\cos\theta$ is strictly geometrical in nature and independent of any arbitrary constants. Curves of $G(\psi,\theta)/\cos\theta$, as calculated from Eqs. (21) are presented in Fig. 7. The abscissa is the reflection angle θ and the curve parameter is the incidence angle ψ. Fig. 7 pertains to the plane of incidence such that ψ_p and θ_p can be replaced by ψ and θ, respectively. Similar curves for a range of azimuthal angles ϕ are presented later.

The striking feature of the results displayed in Fig. 7 is the great increase of $G/\cos\theta$ as θ approaches $+90°$. This increase is accentuated with increasing incidence angle ψ. Such an increase is necessary for the occurrence of off-specular peaks. The curves also exhibit local maxima at negative θ-values. These are quite similar to the local maxima shown by the experimental results for aluminum in Fig. 2(a) for $\psi=45°$, 60°, and 75°. It is thus evident that the quantity $G/\cos\theta$, as formulated here, possesses a dependence on ψ and θ which is suggestive of the experimental data.

The application of the multiplicative exponential factor of expression (24) will now be discussed. In working graphs, the function $[G(\psi,\theta)/\cos\theta]\exp(-c^2\alpha^2)$ was plotted for values of the paramenter c ranging from 0.01 to 0.20. The resulting curves were appraised on the basis of how well they predicted the growth of the off-specular peaks shown in Fig. 2. A value of $c=0.05$ was judged best, although a change of c by ±0.01 does not appreciably alter the distributions. The appropriate value of c may well be different for other materials and other surface roughnesses. However, the foregoing choice of $c=0.05$ is substantiated

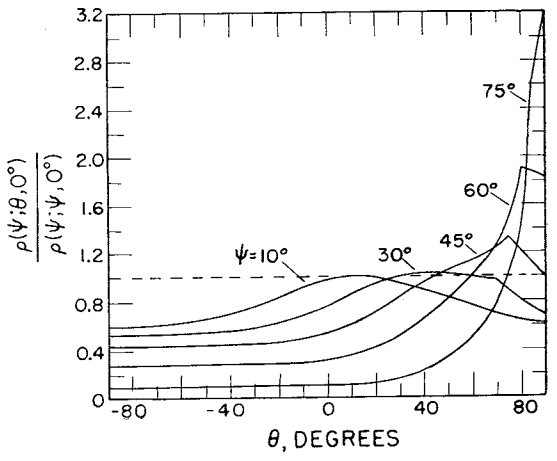

FIG. 8. Bidirectional reflectance distributions in the plane of incidence for various incidence angles ψ as calculated from Eq. (23). $F(\psi',\hat{n})=1$, $c=0.05$, and $g=\frac{2}{3}$.

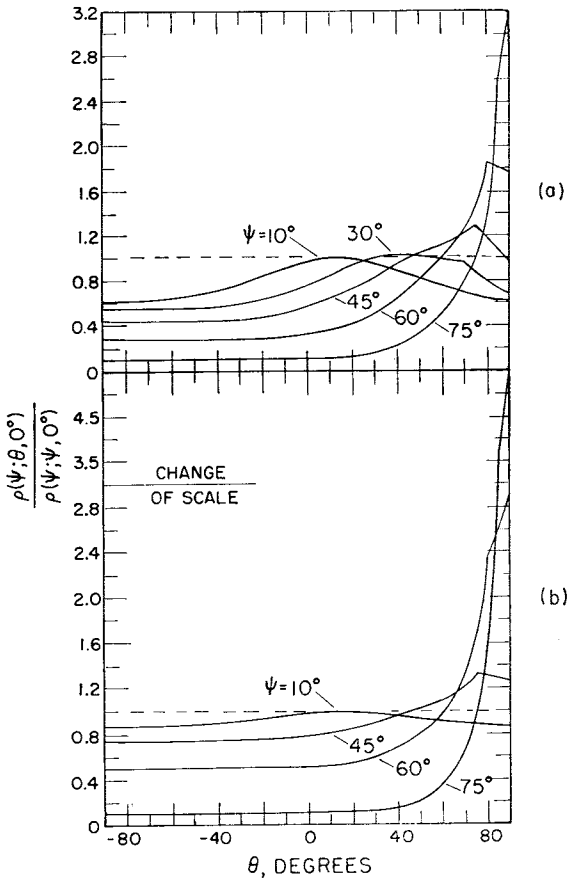

FIG. 9. Predicted bidirectional reflectance distributions corresponding to the experimental distributions in Fig. 2. Calculated from Eq. (23) with $c=0.05$ and $F(\psi',\hat{n})$ evaluated at $\lambda=0.5\ \mu$. (a) Aluminum, $g=\frac{2}{3}$. (b) Magnesium oxide, $g=2$.

by experimentally-determined values of 0.035 and 0.046 reported for ground glass surfaces.[23]

The bidirectional reflectance ratio expressed by Eq. (23) was then evaluated for various g values with the Fresnel reflectance $F(\psi',\hat{n})$ set equal to unity. This avoids having to introduce the material properties of the surface. In order that the level of the calculated curves agree with the experimental curves for both materials in Fig. 2 when $\psi=75°$, a value of $g=\frac{2}{3}$ was selected. The predictions of Eq. (23) corresponding to $c=0.05$, $g=\frac{2}{3}$ and $F=1$ are shown in Fig. 8.

The calculated distributions pictured in Fig. 8 closely resemble the experimental curves in Fig. 2. The curves in Fig. 8, however, exhibit neither the sharp drop-off at large positive θ-values (beyond the off-specular peak) nor the local maxima at negative θ-values that are shown by the experimental curves for aluminum. The former deficiency is attributable to idealizations in the model used for the masking-shadowing effect, while the latter can be attributed to the assumed gaussian facet-slope distribution. It can be shown that a modified gaussian distribution which tends toward a constant value rather than to zero as

α increases would permit the back peaks of Fig. 7 to persist in a presentation similar to Fig. 8. Such a modification did not appear to have a firm justification and was not pursued further.

Fig. 9 shows the effect of introducing the appropriate Fresnel reflectance into Eq. (23). New constants g were chosen so that $g \cdot F(\psi=75°, \hat{n}) \approx \frac{2}{3}$ for the two materials (a g value of $\frac{2}{3}$ had been used in Fig. 8.) The Fresnel reflectance curve for aluminum does not vary significantly throughout its angular range, but the Fresnel curve for magnesium oxide varies considerably. Consequently, the curves in Figs. 8 and 9(a) differ only slightly, while the curves in Figs. 8 and 9(b) show significant differences. Indeed, in the latter, the magnitudes of the off-specular peaks and the values at $\theta=0°$ are now in better accord with experiment.

The over-all agreement between the corresponding curves of Figs. 2 and 9 lends strong support to the general validity of the present analytical model for $\sigma_m/\lambda > 1$. As σ_m/λ decreases to values less than unity, the approach to specular reflection must be explained by a model based on physical optics.

For the sake of completeness, the factor $G(\psi_p,\theta_p)/\cos\theta$ and the relative bidirectional reflectance of Eq. (23) were evaluated for various azimuthal angles ϕ out of the plane of incidence. For this purpose, $c=0.05$, $g=\frac{2}{3}$, and $F=1$. The results are presented in Figs. 10 and 11 for three incidence angles, $\psi=30°$, 60°, and 75°. These figures display the transition between results for $\phi=0°$ and $\phi=180°$ that have already been presented in Figs. 7 and 8. It is evident that for each incidence angle ψ, a smooth transition of angular distributions takes place as ϕ ranges from 0° to 180°. These figures thus illustrate the diminution of the off-specular peaks as the azimuthal orientation departs more and more from $\phi=0°$.

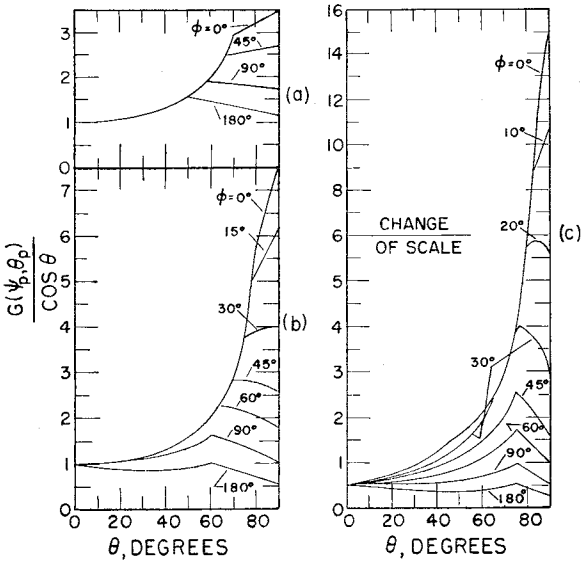

FIG. 10. The factor $G(\psi_p,\theta_p)/\cos\theta$ for various azimuthal angles ϕ. (a) $\psi=30°$. (b) $\psi=60°$. (c) $\psi=75°$.

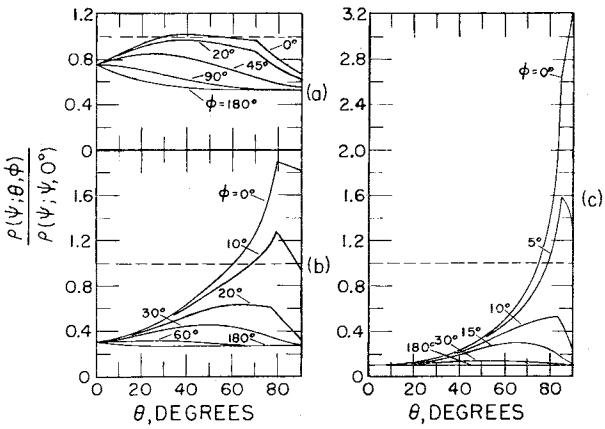

FIG. 11. Bidirectional reflectance distributions for various azimuthal angles ϕ as predicted by Eq. (23). $F(\psi',\hat{n})=1$, $c=0.05$, and $g=\frac{2}{3}$. (a) $\psi=30°$. (b) $\psi=60°$. (c) $\psi=75°$.

CONCLUDING REMARKS

An analytical model for reflection by roughened surfaces has been proposed and evaluated. The model pictures the surface as consisting of small randomly-disposed mirror-like facets. Specular reflection from these facets plus a diffuse component due to multiple reflections and/or internal scattering are assumed to be the basic mechanisms of reflection. The effects of shadowing and masking of facets by adjacent facets are included. The analysis employs only geometrical optics and applies when the surface roughness-to-wavelength ratio (σ_m/λ) is greater than unity. The mathematical formulation of these processes leads to Eq. (23) for the angular distribution of the bidirectional reflectance ratio. This relation predicts off-specular peaks which emerge as the angle of incidence is increased. The analytical predictions are in very good agreement with experimentally determined angular distributions for both metal and nonmetal surfaces.

The model thus affords an explanation for the off-specular peak phenomenon in terms of the mirror-like surface facets. Specular reflection from these facets causes the radiance of the reflected flux to increase markedly with increasing zenith angles of reflection (measured relative to the mean-surface plane). This great reflected radiance is attenuated at near-grazing reflection angles by masking and shadowing of facets by adjacent facets. The net result of these processes is to cause off-specular peaks such as those observed experimentally.